

# 1 Photoproduction of nitric oxide in seawater

2 Ye Tian<sup>1,2,3</sup>, Gui-Peng Yang<sup>1,2,3</sup>, Chun-Ying Liu<sup>1,2,3</sup>, Pei-Feng Li<sup>3</sup>, Hong-Tao  
3 Chen<sup>1,2,3</sup>, Hermann W. Bange<sup>4</sup>

4 <sup>1</sup>Key Laboratory of Marine Chemistry Theory and Technology, Ministry of Education, Qingdao, 266100,  
5 China

6 <sup>2</sup>Laboratory for Marine Ecology and Environmental Science, Qingdao National Laboratory for Marine  
7 Science and Technology, Qingdao 266071, China

8 <sup>3</sup>College of Chemistry and Chemical Engineering, Ocean University of China, Qingdao, 266100, China

9 <sup>4</sup>GEOMAR Helmholtz-Zentrum für Ozeanforschung Kiel, Kiel, 24105, Germany

10 *Correspondence to:* Chun-ying Liu ([roseliu@ouc.edu.cn](mailto:roseliu@ouc.edu.cn)) and Hong-Tao Chen ([chenht@ouc.edu.cn](mailto:chenht@ouc.edu.cn))

11 **Abstract.** Nitric oxide (NO) is a short-lived intermediate of the oceanic nitrogen cycle. However, our  
12 knowledge about its production and consumption pathways in oceanic environments is rudimentary. In  
13 order to decipher the major factors affecting NO photochemical production, we irradiated artificial  
14 seawater samples as well as 31 natural surface seawater samples in laboratory experiments. The seawater  
15 samples were collected during a cruise to the western tropical North Pacific Ocean (WTNP, a N/S section  
16 from 36 ° to 2 °N along 146 °/143 °E with 6 and 12 stations, respectively, and a W/E section from 137 °  
17 to 161 °E along the equator with 13 stations) from November 2015 to January 2016. NO photoproduction  
18 rates from dissolved nitrite in artificial seawater showed increasing trends with decreasing pH, increasing  
19 temperatures and increasing salinity. In contrast, NO photoproduction rates (average:  $0.5 \pm 0.2 \times 10^{-12}$   
20  $\text{mol L}^{-1} \text{s}^{-1}$ ) in the natural seawater samples from the WTNP did not show any correlations with pH,  
21 water temperature and salinity as well as dissolved inorganic nitrite concentrations. The flux induced by  
22 NO photoproduction in the WTNP (average:  $13 \times 10^{-12} \text{ mol m}^{-2} \text{ s}^{-1}$ ) were significantly larger than the  
23 NO air-sea flux densities (average:  $1.8 \times 10^{-12} \text{ mol m}^{-2} \text{ s}^{-1}$ ) indicating a further NO loss process in the  
24 surface layer.

## 25 1 Introduction

26 Nitric oxide (NO) is a short-lived intermediate of the oceanic nitrogen cycle, see e.g. Bange (2008) and  
27 Kuypers et al. (2018). There are only a few reports about oceanic NO determination method so far  
28 because of its reactivity (Zafiriou et al., 1980; Lutterbeck and Bange, 2015; Liu et al., 2017). NO is  
29 produced and consumed during various microbial processes such as nitrification, denitrification and

30 anammox (Schreiber et al., 2012; Kuypers et al., 2018). Moreover, it is known that both phytoplankton  
 31 and zooplankton can metabolize NO and are influenced by ambient (extracellular) NO concentrations  
 32 (Singh and Lal, 2016; Wang et al., 2017; Astier et al., 2018).

33 Apart from (micro)biological processes, NO can be produced photochemically from dissolved nitrite  
 34 ( $\text{NO}_2^-$ ) in the sunlit surface ocean (Zafiriou and True, 1979; Zafiriou and McFarland, 1981):



36 Mack and Bolton (1999) had reviewed the possible subsequent reaction like the produced NO and  
 37 hydroxyl radical (OH) could react to produce  $\text{HNO}_2$  reversely (R2), and some reaction that consumed  
 38 NO like R3 to R7



45 besides, in natural sunlit seawater, photolyzed dissolved nitrate ( $\text{NO}_3^-$ ) could be a potential source of NO  
 46 through  $\text{NO}_2^-$  (R 8); during the process of ammonium ( $\text{NH}_4^+/\text{NH}_3$ ) oxidation into  $\text{NO}_2^-$  and  $\text{NO}_3^-$ , NO  
 47 might be an intermedium (Joussotdubien and Kadiri, 1970), or NO could be produced through amino-  
 48 peroxy radicals ( $\text{NH}_2\text{O}_2^-$ ) through R 8 to R 11 (Laszlo et al., 1998; Clarke et al., 2008)



55 Table 1 summarized studies about photochemical production of NO measured in the surface waters of  
 56 the equatorial Pacific Ocean (Zafiriou et al., 1980; Zafiriou and McFarland, 1981), the Seto Inland Sea  
 57 (Olasehinde et al., 2009; Olasehinde et al., 2010; Anifowose and Sakugawa, 2017), the Bohai and Yellow  
 58 Seas (Liu et al., 2017; Tian et al., 2018) and the Kurose River (Japan) (Olasehinde et al., 2009; Anifowose

59 et al., 2015). NO photoproduction rates varied among different seawater samples, it seemed the rates in  
60 Kurose River (average:  $499 \times 10^{-12} \text{ mol L}^{-1} \text{ s}^{-1}$ ) was biggest, which was possibly due to an increase of  
61 nitrite being released into the river in agricultural activity during the study time. However, NO  
62 concentration was about  $1.6 \times 10^{-12} \text{ mol L}^{-1}$ , at lowest level, which was because of higher scavenging  
63 rate in river water (NO lifetime :0.25 s). The lifetime of NO showed increasing trend from river (several  
64 seconds) to inland sea (dozens of seconds) to open sea (dozens to hundreds of seconds), reviewed in  
65 Anifowose and Sakugawa (2017). However, NO showed higher concentration level in coastal waters  
66 than in open sea, higher photoproduction rates might account for this.

67 In this study, we present the results of our measurements of NO photoproduction in laboratory  
68 experiments using artificial and natural seawater samples. The major objectives of our studies were (i)  
69 to decipher the factors affecting NO photoproduction in seawater, (ii) to determine the photoproduction  
70 rates of NO from samples collected during a cruise to the western tropical North Pacific Ocean (WTNP)  
71 and (iii) to quantify the role of photoproduction as a source of NO in the surface waters of the WTNP.

## 72 **2 Methods**

### 73 **2.1 Determination of dissolved NO in aqueous samples**

74 For the measurements of dissolved NO we applied the method described by Olasehinde et al. (2009): In  
75 brief, NO in the aqueous samples was determined by trapping it with added 4,5-diaminofluorescein  
76 (DAF-2, chromatographic grade from Sigma-Aldrich, USA) and measuring the reaction product  
77 triazolo fluorescein (DAF-2T) with a high performance liquid chromatography system (HPLC). We used  
78 an Agilent 1260 Infinity HPLC (Agilent Technologies Inc., USA) system equipped with a Venusil XBP-  
79 C18 column (5.0  $\mu\text{m}$ ; 4.6 mm  $\times$  250 mm i.d.). The column temperature was set to 25°C and the mobile  
80 phase was comprised of acetonitrile (HPLC grade from Merck, Darmstadt, Germany) and phosphate  
81 buffer (disodium hydrogen phosphate heptahydrate, guaranteed reagent from Sinopharm Chemical  
82 Reagent Co., Ltd, Shanghai, China) solution (10 mmol L<sup>-1</sup> at pH 7.4) with a ratio of 8:92 (v:v) and a flow  
83 rate of 1 mL min<sup>-1</sup> in the isocratic mode.

84 The injected sample volume was 5.0  $\mu\text{L}$ . The eluate was analyzed with a fluorescence diode array  
85 detector at wavelengths of 495 and 515 nm for excitation and emission, respectively. The retention time  
86 of DAF-2T was about 5.5 min.

87 An aliquot of 10 mL artificial seawater was bubbled with N<sub>2</sub> gas at a flow of 10 mL min<sup>-1</sup> for 2 h to  
88 remove O<sub>2</sub> after 10 min of ultrasonic and heat degassing. The solution was then bubbled with high-purity  
89 NO gas (99.9 %, Dalian Date Gas Ltd., China) for 30 min. The concentration of the saturated NO stock  
90 solution was 1.4 mmol L<sup>-1</sup>, which could be used within 3 h (Lantoine et al., 1995). A series of diluted  
91 NO solutions were prepared in N<sub>2</sub>-purged water from the NO stock solution using a microsyringe (Xing  
92 et al., 2005; Liu et al., 2017). And the series samples were trapped by DAF-2 solution.  
93 The detection limit of dissolved NO in Milli-Q water was 9.0×10<sup>-11</sup> mol L<sup>-1</sup>, which was determined by  
94 S/N=3 (3×0.03) with the blank samples (n=7) and the slope (0.101) in the low concentration range (3.3  
95 – 33×10<sup>-10</sup> mol L<sup>-1</sup>). And average relative standard error of the NO measurements was +/- 5.7 % at a  
96 concentration of 3.0 × 10<sup>-9</sup> mol L<sup>-1</sup>.

## 97 **2.2 Set-up of irradiation experiments**

98 We performed irradiation experiments with Milli-Q water (18.2 MΩ cm, Millipore Company, USA),  
99 artificial seawater and natural seawater samples. Artificial seawater was prepared by dissolving 23.96 g  
100 NaCl, 5.08 g MgCl<sub>2</sub>, 3.99 g Na<sub>2</sub>SO<sub>4</sub>, 1.12 g CaCl<sub>2</sub>, 0.67 g KCl, 0.20 g NaHCO<sub>3</sub>, 0.10 g KBr, 0.03 g  
101 H<sub>3</sub>BO<sub>3</sub> and 0.03 g NaF in 1 L of Milli-Q water (Bajt et al., 1997) and filtered by 0.2 μm polyethersulfone  
102 membrane (Pall, USA) before the experiments.

103 All irradiation experiments (except the experiments for the temperature dependence, see section below)  
104 were conducted at a constant temperature of 20 °C by controlling the temperature of thermostat water  
105 bath (LAUDA Dr. R. Wobser GmbH & Co. KG, Germany). The height of cylindroid quartz cuvette used  
106 for irradiation was 70 mm and the inner diameter was 14 mm with the volume about 10 mL. The optical  
107 pathlength was about 70 mm. During the experiment, the quartz cuvette, filled with 10 mL sample and  
108 blocked by PTFE stopper, was installed in the simulator and a little higher than the water bath surface.  
109 All quartz cuvettes were treated in the same manner except the cuvettes wrapped in aluminum foil which  
110 served as dark control.

111 Milli-Q water and artificial seawater samples were spiked with varying amounts of NaNO<sub>2</sub> (puriss. p.a.  
112 ACS grade from Sigma-Aldrich, USA; for details see sections below). All other chemicals were of  
113 analytical grade from Tianjin Kemiou Chemical Reagent Co., Ltd or Shanghai Sinopharm Chemical  
114 Reagent Co., Ltd.

115 Triplicate samples from each treatment were collected every 0.5 h with an entire irradiation time of 2 h.  
116 At the sampling time, the SUNTEST CPS+ was turned off and triplicate subsamples were collected from  
117 each sample in dark with microsyringe (50  $\mu\text{L}$ ), and then the cuvettes were quickly put back into the  
118 water bath to continue the experiment until two hours. The data from the experiments with Milli-Q and  
119 artificial seawater samples were fitted with a simple linear regression in artificial seawater samples (see  
120 below). However, a linear relationship was not found  $> 30$  min for the natural seawater samples, therefore,  
121 we decided to choose 30 min as the total experimental time for natural seawater samples. Statistical  
122 analyses were done using SPSS v.16.0 or Origin 9.0 and results were considered significant at  $p \leq 0.05$ .  
123 The artificial light source was a 1.5 kW xenon lamp, which provided a light intensity of  $765 \text{ W m}^{-2}$ . The  
124 lamp was installed in an immersion well photochemical reactor called SUNTEST CPS+ solar simulator  
125 produced by ATLAS, Germany. The solar simulator employed in this study has been demonstrated to  
126 produce spectra which mimics that of the solar radiation and emits a radiation of wavelength from 300  
127 to 800 nm (Wu et al., 2015).

## 128 **2.3 Experimental outline**

### 129 **2.3.1 Optimal DAF-2 concentration and storage time**

130 In order to find out the optimal DAF-2 concentration, 10 mL of artificial seawater containing  $0.5 \mu\text{mol}$   
131  $\text{L}^{-1} \text{NO}_2^-$  was irradiated with various concentrations of DAF-2 ranging from  $0.7 \mu\text{mol L}^{-1}$  to  $4.8 \mu\text{mol}$   
132  $\text{L}^{-1}$  for 2 h.

133 To ascertain the sample storage time, 10 mL with artificial seawater samples containing  $5.0 \mu\text{mol L}^{-1}$  or  
134  $0.5 \mu\text{mol L}^{-1} \text{NO}_2^-$  were irradiated with various concentrations of DAF-2 for 2 h. After irradiation,  
135 samples were kept in the dark and measured every 2 h.

### 136 **2.3.2 Influence of pH, temperature, salinity and wave lengths**

137 The influence of the pH was assessed by adjusting artificial seawater samples to pH levels of 7.1, 7.6  
138 and 8.1 by addition of appropriate amounts of hydrochloric acid ( $2 \text{ mol L}^{-1}$ ) or caustic soda solution ( $2$   
139  $\text{mol L}^{-1}$ ).

140 To assess the influence of the temperature, artificial seawater samples were adjusted to temperatures of  
141  $10 \text{ }^\circ\text{C}$ ,  $20 \text{ }^\circ\text{C}$  and  $30 \text{ }^\circ\text{C}$  by controlling the temperature of the thermostat water bath.

142 To assess the influence of the salinity on the photoproduction of NO from dissolved  $\text{NO}_2^-$ , artificial  
143 seawater samples were adjusted to different salinity of 20, 30 and 35 by adding Milli-Q water or NaCl  
144 to the stock solution of artificial seawater.

145 In order to compare the contributions of ultraviolet A (UVA), ultraviolet B (UVB) and visible light to  
146 the NO photoproduction, two kinds of light filter film were used (wrapped around the quartz cuvette  
147 tubes: (i) a Mylar plastic film (from United States Plastic Cor., Lima, Ohio) which can only shield UVB  
148 and (ii) a film, always used as car insulation film (from CPFilm Inc., USA) shielding both UVA and  
149 UVB (Li et al., 2010; Wu et al., 2015).

#### 150 **2.4 Calculations of photoproduction rates ( $R_{\text{NO}}$ ), photoproduction rate constant ( $J_{\text{NO}}$ ) and reaction** 151 **yield**

152 For the artificial seawater experiments determining the generation of NO from the  $\text{NO}_2^-$  photochemical  
153 degradation, the data fitted with a simple linear regression with the form  $y = R_{\text{NO}} \times t + b$ , where  $y$  is the  
154 NO concentration which was calculated by the signal intensity of DAF-2T at time  $t$  and  $R_{\text{NO}}$  is the  
155 photoproduction rate.

156 The photoproduction rate constant of NO from nitrite ( $J_{\text{NO}}$ ) was determined by preparing different  
157 concentrations of  $\text{NO}_2^-$  (0.5, 2.0 and 5.0  $\mu\text{mol L}^{-1}$ ) in Milli-Q water and artificial seawater. The slope of  
158 the linear correlation between photoproduction rates and concentrations of  $\text{NO}_2^-$  represents  $J_{\text{NO}}$   
159 (Anifowose et al., 2015).

160 The yield of NO formation ( $\%f_{\text{NO}}$ ) from the photodegradation via  $\text{NO}_2^-$  was estimated according to  
161 Anifowose et al. (2015)

$$162 \quad \%f_{\text{NO}} = 100 \times J_{\text{NO}} \times c(\text{NO}_2^-) \times R_{\text{NO}}^{-1} \quad (\text{Eq 1})$$

163 where  $c(\text{NO}_2^-)$  is the initial concentration of  $\text{NO}_2^-$ .

#### 164 **2.5 Seawater samples**

165 Surface seawater samples were collected from a water depth of 1 m during a ship campaign to the western  
166 tropical North Pacific Ocean on board the R/V “Dong Fang Hong 2” from 13 November 2015 to 5  
167 January 2016. This cruise covered two sections: a N/S section from 36 to 2°N along 146/143°E with 6  
168 and 12 stations, respectively, and a W/E section from 137 to 161°E along the equator with 13 stations  
169 (Fig. 1). Stations S0701 – S0723 were sampled between 11 and 28 November (i.e. the first part of the  
170 N/S section), followed by sampling of W/E section between 16 and 27 December and sampling of

171 stations S0725 – S0735 between 30 December 2015 and 05 January 2016 (i.e. second part of the N/S  
172 section). In addition, relevant surface currents are indicated in Fig. 1 (Fine et al., 1994; Zhao et al., 2016;  
173 Zhang et al., 2018). The location of the Kuroshio Current on 15 November 2015 was taken from  
174 <https://www1.kaiho.mlit.go.jp/>.

175 Seawater samples were collected using 8-liter Niskin bottles equipped with silicon O-rings and Teflon-  
176 coated springs and mounted on a Sea-Bird CTD (conductivity, temperature, depth) instrument (Sea-Bird  
177 Electronics, Inc., USA). A 750 mL black glass bottle was rinsed with in situ seawater three times, and  
178 then was filled with seawater quickly through a siphon. When the overflowed sample reached the half  
179 volume of the bottle, the siphon was withdrawn rapidly, and the bottle was sealed quickly. Samples were  
180 filtered through 0.45 µm and 0.2 µm polyethersulfone membranes (Pall, USA) to minimize microbial  
181 influence (Kieber et al., 1996; Yang et al., 2011). Then the filtered seawater was transferred in the dark  
182 into acid-cleaned and pre-combusted amber glass bottles, stored in darkness at 4 °C and brought back to  
183 the laboratory on land. Samples were re-filtered with 0.2 µm polyethersulfone membranes (Pall, USA)  
184 before the irradiation experiments. DAF-2 solutions were added in the dark. The irradiation experiments  
185 were conducted within two weeks after the samples arrived in the land laboratory, the maximum storage  
186 time was about two months.

## 187 **2.6 Dissolved inorganic nitrogen (DIN) and pH measurements**

188 The concentrations of dissolved inorganic nitrogen (DIN = nitrate, nitrite, and ammonium) from the  
189 cruise were analyzed using an automated nutrient analyzer (SKALAR San++ system, SKALAR,  
190 Netherlands) onboard. The detection limits were 0.05 µmol L<sup>-1</sup> for nitrate, nitrite and ammonium. When  
191 the concentration was below detection limit,  $\frac{1}{2}$  of the detection limit (0.025 round-off to 0.02) was  
192 used.

193 The pH values were measured just before the experiments by using a benchtop pH meter (Orion Star  
194 A211, Thermo Scientific <sup>TM</sup>, USA) which was equipped with an Orion 8102 Ross combination pH  
195 electrode (Thermo Scientific <sup>TM</sup>, USA). In order to ensure comparability with the temperature in the  
196 irradiation experiments, pH values of the natural seawater samples were measured at 20 °C. The pH meter  
197 was calibrated with three NIST-traceable pH buffers (pH = 4.01, 7.00 and 10.01 at 20 °C). The precision  
198 of pH measurements was +/-0.01.

## 199 **3 Results and Discussion**

### 200 **3.1 Optimal DAF-2 concentration and storage time**

201 NO concentrations generated from photolysis of artificial seawater samples with an initial  $\text{NO}_2^-$   
202 concentration of  $0.5 \mu\text{mol L}^{-1}$  increased with increasing DAF-2 concentrations and reached a maximum  
203 at a DAF-2 concentration of  $1.4 \mu\text{mol L}^{-1}$  (Fig. 2a). At DAF-2 concentrations  $>1.4 \mu\text{mol L}^{-1}$  no further  
204 increase of the NO concentrations was observed. Thus, we used a DAF-2 concentration of  $1.4 \mu\text{mol L}^{-1}$   
205 for all experiments.

206 Samples after reaction with DAF-2 and stored at  $4^\circ\text{C}$  in the dark were stable for at least 28 h with the  
207 measurement interval about 2 h (Fig. 2b). The relative standard deviations of the resulting NO  
208 concentrations after irradiating samples containing  $0.5 \mu\text{mol L}^{-1}$  and  $5.0 \mu\text{mol L}^{-1}$   $\text{NO}_2^-$  were  $\pm 13\%$   
209 and  $\pm 7\%$ , respectively. This demonstrated that photolysis samples with NO which were allowed to  
210 react with DAF-2 could be stored for at least one day at  $4^\circ\text{C}$  in the dark.

### 211 **3.2 Photoproduction of NO in Milli-Q water and artificial seawater**

212 The photoproduction rates of NO in samples with  $\text{NO}_2^-$  concentrations of 0.5, 2.0 and  $5.0 \mu\text{mol L}^{-1}$  were  
213 generally higher in artificial seawater than in Milli-Q water (Fig. 3a and 3b).

214 The resulting  $J_{\text{NO}}$  were  $5.6 \pm 0.9 \times 10^{-4} \text{ min}^{-1}$  and  $9.4 \pm 1.4 \times 10^{-4} \text{ min}^{-1}$  for Milli-Q water and artificial  
215 seawater, respectively. They are lower than the  $J_{\text{NO}}$  of  $34.2 \times 10^{-4} \text{ min}^{-1}$  for Milli-Q water reported by  
216 Anifowose et al. (2015). The difference might be explained by different experimental set-ups such as  
217 sample self-shading, in our study, the quartz cuvette was 70 mm height and inner diameter was 14 mm  
218 with the volume about 10 mL while in Anifowose et al. (2015), the quartz photochemical reaction cell  
219 was 3 cm in diameter, 1.5 cm in length, and had a 6.5 mL capacity.

### 220 **3.3 Influence of pH, temperature, salinity and wavelengths**

221 All irradiation experiments were conducted in artificial seawater with two different  $\text{NO}_2^-$  concentrations  
222 of 0.5 and  $5.0 \mu\text{mol L}^{-1}$ . The resulting NO concentrations were generally higher when irradiating the  
223 samples with the initial  $\text{NO}_2^-$  concentration of  $5.0 \mu\text{mol L}^{-1}$ . NO photoproduction rates showed  
224 increasing trends with decreasing pH, increasing temperatures and increasing salinity, the relationship  
225 between rates with salinity and temperature rates is significant ( $p < 0.5$ ) (Fig. 4 and 5).



226 Reaction (1) indicates that decreasing pH which results in lower concentrations of OH<sup>-</sup> which, in turn,  
 227 will promote NO formation via NO<sub>2</sub><sup>-</sup>. This is in line with the finding of Li et al. (2011) who found that  
 228 the photodegradation rate of NO<sub>2</sub><sup>-</sup> in Milli-Q water was higher at pH = 6.5 than at pH = 9.5. Tugaoen et  
 229 al. (2018) also found the effect of lowering pH to conjugate NO<sub>2</sub><sup>-</sup> to HONO allowed for HONO  
 230 photolysis (pH = 2.5). Besides, higher pH could also inhibit N<sub>2</sub>O<sub>4</sub> and N<sub>2</sub>O<sub>3</sub> hydrolysis reaction (R4 and  
 231 R7) as reviewed by Mack and Bolton (1999). However in previous study of Chu and Anastasio (2007)  
 232 and Zellner et al. (1990), the quantum yield of OH (which equals to the quantum yield of NO) was  
 233 constant at the pH ranges from 6.0 to 8.0 and 5.0 to 9.0 under single wavelength light in nitrite solution.  
 234 This might indicated that decreasing pH in our study mainly reduced NO consumption rather than  
 235 increased NO production.

236 Higher temperatures led to increasing NO photoproduction rates according to the temperature  
 237 dependence of chemical reactions given by the Arrhenius formula:

$$238 \quad R = A \times \exp\left(-\frac{E}{R \times T}\right) \quad (\text{Eq 2})$$

239 where  $A$  is an Arrhenius prefactor and  $T$  is the temperature (K). This indicates that an increasing  
 240 temperature results in a higher rate, Chu and Anastasio (2007) also found that quantum yield of OH (or  
 241 NO) showed a decreasing trend from 295K, 263K to 240K. Moreover, this equation can be used to  
 242 consider the difference of the rates at two temperatures  $T_1$  and  $T_2$ :

$$243 \quad R_{T_2} = R_{T_1} \times \exp\left(\frac{E}{R} \times \left(\frac{1}{T_1} - \frac{1}{T_2}\right)\right) \quad (\text{Eq 3})$$

244 If we assumed that  $E$  was a constant in the temperature ranges of 10 to 30 °C when NO<sub>2</sub><sup>-</sup> = 0.5 μmol L<sup>-1</sup>,  
 245 and we plot  $\ln R$  against  $1/T$ , we would get the  $E$  value as 57.5 kJ mol<sup>-1</sup> K<sup>-1</sup>. Using the photoproduction  
 246 rate at 20 °C (293.15 K) as our reference point ( $T_1$ ), an expression of the  $R_T$  with the temperature was as  
 247 follows:

$$248 \quad R_T = 2.7 \times 10^{-10} \times \exp\left(6920 \times \left(\frac{1}{293.15} - \frac{1}{T_2}\right)\right) \quad (\text{Eq 4})$$

249 Similarly, we could conclude expression of the  $R_T$  with the temperature when NO<sub>2</sub><sup>-</sup> = 5.0 μmol L<sup>-1</sup>,

$$250 \quad R_T = 7 \times 10^{-10} \times \exp\left(11026 \times \left(\frac{1}{293.15} - \frac{1}{T_2}\right)\right) \quad (\text{Eq 5}).$$

251 However, NO production rate at 0.5 μmol L<sup>-1</sup> nitrite did not increase from 20 to 30 °C, the plausible  
 252 explanation was that NO<sub>2</sub><sup>-</sup> concentration here was the mainly influencing factor, NO<sub>2</sub><sup>-</sup> might be run out

253 at 20 °C, if  $\text{NO}_2^-$  concentration increased, like up to  $5.0 \mu\text{mol L}^{-1}$ , the temperature could make a noticeable  
254 difference.

255 Higher salinity obviously enhanced photoproduction rates of NO in both Milli-Q water and artificial  
256 seawater samples (with  $0.5 \mu\text{mol L}^{-1}$  or  $5.0 \mu\text{mol L}^{-1}$  initial  $\text{NO}_2^-$  concentrations). The regression  
257 relationship is  $y = 0.37 x - 4.55$  for  $0.5 \mu\text{mol L}^{-1} \text{NO}_2^-$  and  $y=2.3 x - 39.5$  for  $5.0 \mu\text{mol L}^{-1} \text{NO}_2^-$ ,  
258 respectively, where x is the salinity (‰) and y is the photoproduction rate ( $\times 10^{-10} \text{mol L}^{-1} \text{s}^{-1}$ ). This result  
259 indicates that with increasing ion strength NO production is enhanced, however, the exact mechanism is  
260 unknown and need further study. Zafiriou and McFarland (1981) also demonstrated that artificial  
261 seawater comprised with major and minor salts showed complex interactions. But Chu and Anastasio  
262 (2007) reported that added  $\text{Na}_2\text{SO}_4$  ( $4.0\text{--}7.0 \text{mmol L}^{-1}$ ) in solution had no effect on the quantum yield of  
263 OH.

264 The highest NO photoproduction rates were observed with full wave length band whereas the lowest NO  
265 rates were observed with UVB. The NO photoproduction rates approached zero at wave lengths in the  
266 visible band. The contribution of visible band, UVA band and UVB band were  $<1\%$ ,  $30.7\%$ ,  $85.2\%$  and  
267  $<1.0\%$ ,  $34.2\%$ ,  $63.1\%$  for  $0.5$  and  $5.0 \mu\text{mol L}^{-1} \text{NO}_2^-$ , respectively. Our results are in line with the  
268 findings of Zafiriou and McFarland (1981) who found that samples exposed to (UV+visible) wave  
269 lengths lost  $\text{NO}_2^-$  more rapidly than those exposed only to the visible wave lengths alone. Chu and  
270 Anastasio (2007) found that under single wavelength light, quantum yield of OH decreased with the  
271 wavelength (280 nm to 360 and plateau until 390) which meant that single wavelength light of UVB had  
272 higher photoproduction rate than UVA. Since it might be because of the wild band of UVA (320–420  
273 nm) that led to the summational higher rates under UVA than UVB (in our system 300-320). Moreover,  
274 according to the UV–visible absorption spectra of  $\text{NO}_2^-$ ,  $\lambda_{\text{max}}$  was 354 nm, which is in the range of UVA  
275 (320–420 nm) (Zuo and Deng, 1998; Zafiriou and McFarland, 1981).

### 276 **3.4 Kinetics of the NO photoproduction**

277 The yields of NO formation from  $\text{NO}_2^-$  ( $\%f_{\text{NO}}$ ) in artificial seawater samples were about  $70.1\%$  and  $97.9\%$   
278 for the initial  $\text{NO}_2^-$  concentrations of  $0.5$  and  $5.0 \mu\text{mol L}^{-1}$ , respectively. The missing NO yield ( $29.9\%$   
279 for  $0.5 \mu\text{mol L}^{-1}$  and  $2.1\%$  for  $5.0 \mu\text{mol L}^{-1}$ ) might result from NO production via other (unknown)  
280 nitrogen-containing substrates (Anifowose et al., 2015). Another plausible explanation would be that  
281 during the process of  $\text{NO}_2^-$  photoproduction, some NO were oxidized into  $\text{NO}_2$ , then  $\text{NO}_2$  dimerized (R5)

282 and the dipolymer  $\text{N}_2\text{O}_4$  would hydrolyze into  $\text{NO}_2^-$  and  $\text{NO}_3^-$  (R7), which actually reduce the  
283 concentration of  $\text{NO}_2^-$  (Mack and Bolton, 1999).

284 Assuming a 100% yield from  $\text{NO}_2^-$  degradation and a fast reaction of NO with DAF-2 the observed  
285 linear relationships during the various irradiation experiments (Fig. 6) indicate that NO photoproduction  
286 was following a pseudo zero-order reaction. However, the  $R_{\text{NO}}$  ratios (average: 4.8) listed in Table 2  
287 were not the same for the experiments despite the fact that the ratio of the initial  $\text{NO}_2^-$  concentrations (=   
288 10) was the same for all experiments. This result, however, does point to reaction which is different from  
289 a zero-order reaction.

### 290 **3.5 Photoproduction rates of NO in the western tropical North Pacific Ocean**

291 During the cruise surface temperatures and salinities were in the range from 22.15 °C to 30.19 °C and  
292 34.57 to 35.05 respectively. The concentrations of  $\text{NO}_3^-$ ,  $\text{NH}_4^+$  and  $\text{NO}_2^-$  ranged from 0.03  $\mu\text{mol L}^{-1}$  to  
293 1.6  $\mu\text{mol L}^{-1}$ , 0.20  $\mu\text{mol L}^{-1}$  to 1.2  $\mu\text{mol L}^{-1}$  and 0.02  $\mu\text{mol L}^{-1}$  to 0.33  $\mu\text{mol L}^{-1}$ , respectively (Fig. 6).  
294 The measured photoproduction rates of NO ranged from  $0.3 \times 10^{-10} \text{ mol L}^{-1} \text{ min}^{-1}$  (station S0711) to  $2.9$   
295  $\times 10^{-10} \text{ mol L}^{-1} \text{ min}^{-1}$  (station S0303), with an average value of  $13.0 \pm 7.6 \times 10^{-11} \text{ mol L}^{-1} \text{ min}^{-1}$ .  
296 Photoproduction rates did not show significant correlations with  $\text{NO}_2^-$ ,  $\text{NO}_3^-$ ,  $\text{NH}_4^+$ , pH, salinity, water  
297 temperature as well as with colored dissolved organic matter (data not shown, the same method with Zhu  
298 et al. (2017))(statistics computed with SPSS v.16.0).

299 The non-existing linear relationship between  $R_{\text{NO}}$  and dissolved  $\text{NO}_2^-$  during our cruise is in contrast to  
300 the results of Olasehinde et al. (2010), Anifowose et al. (2015) and Anifowose and Sakugawa (2017)  
301 who observed positive linear relationships between NO photoproduction rates and the  $\text{NO}_2^-$   
302 concentrations in the surface waters of the Seto Inland Sea and the Kurose River. This might be because  
303 that other factors like pH, salinity were different between samples collected at different stations.

304 In Table 1, we found that the average photoproduction rate of NO measured in our cruise is lower than  
305 that of the Seto Inland Sea and the Kurose River which could be ascribed to higher background  $\text{NO}_2^-$  in  
306 the inland sea waters (Olasehinde et al., 2009; 2010). Our result is slightly lower than the  $R_{\text{NO}}$  from the  
307 central equatorial Pacific Ocean ( $> 10^{-12} \text{ mol L}^{-1} \text{ s}^{-1}$ ), the lower concentration of  $\text{NO}_2^-$  (0.06  $\mu\text{mol L}^{-1}$ )  
308 in our study area might account for this (Zafiriou and McFarland, 1981). In Table 1, the  $\text{NO}_2^-$   
309 concentration of 0.06  $\mu\text{mol L}^{-1}$  in our study was lower than most of other study area like Qingdao coastal  
310 waters (0.75  $\mu\text{mol L}^{-1}$ ) and the Seto Inland Sea (0-0.4  $\mu\text{mol L}^{-1}$  or 0.5-2  $\mu\text{mol L}^{-1}$ ). In the study of

311 Anifowose et al. (2015), since the  $\text{NO}_2^-$  concentration of upstream K1 station was similar to ours (0.06  
 312  $\mu\text{mol L}^{-1}$ ), the higher  $R_{\text{NO}}$  might attributed to lower pH (7.36) as mentioned above. Or it might be because  
 313 the difference of the river water and the seawater, considering lower nitrite level of K1, dissolved organic  
 314 matter might also account for the higher  $R_{\text{NO}}$ . Because of its conservative mixing behavior with salinity,  
 315 dissolved organic matter always showed higher level in river than open sea (Zhu et al., 2017), which  
 316 could photodegrade itself to produce  $\text{NO}_2^-$ , finally to promote  $R_{\text{NO}}$ . In our study, the rates were adjusted  
 317 to the ambient conditions, which included nighttime samples when the rates were lower. From the T–S  
 318 diagram (Fig.7), we found that higher photoproduction rates at stations S0701 and S0704 might resulted  
 319 from the influence of the Kuroshio (see Fig. 1), with enhanced concentrations of  $\text{NO}_2^-$ . The higher NO  
 320 production rates measured for stations S0303/S0307 and S0717–S0723 might have been influenced by  
 321 the South Equatorial and North Equatorial Currents, respectively, but were obviously not associated with  
 322 enhanced  $\text{NO}_2^-$  concentrations.

323 If we take the missing 30% of  $f_{\text{NO}}$  in artificial seawater as the experimental error, then in our study, using  
 324 the  $J_{\text{NO}}$  in the artificial seawater, the average % $f_{\text{NO}}$  value in natural water was calculated to be 52% (  
 325 30%), indicating that there are other unknown nitrogenous compounds, for example,  $\text{NO}_2^-$  produced from  
 326  $\text{NO}_3^-$  photolysis (R8) or from other organic matter which could further lead to NO production (Kieber et  
 327 al., 1999; Benedict et al., 2017; Goldstein and Rabani, 2007; Minero et al., 2007).

328 According to the photoproduction rates and the relevant  $\text{NO}_2^-$  in Olasehinde et al. (2010), Anifowose  
 329 and Sakugawa (2017) (Table 1), the photoproduction rates under lower than  $0.02 \mu\text{mol L}^{-1} \text{NO}_2^-$  might  
 330 not be determined in nearshore waters like the Seto Inland Sea.

### 331 **3.6 Flux densities of NO in the surface layer of the WTNP**

#### 332 **3.6.1 Air–sea flux density of NO**

333 The NO flux densities were computed with (Eq 6):

$$334 \quad F = k_{sea} ([\text{NO}] - p\text{NO}_{\text{air}} \times H^{cp}) \quad (\text{Eq 6})$$

$$335 \quad p\text{NO}_{\text{air}} = x'\text{NO}_{\text{air}} \times (p_{ss} - p_w) \quad (\text{Eq 7})$$

336 here  $F$  stands for the flux density ( $\text{mass area}^{-1} \text{time}^{-1}$ ) across the air–sea interface,  $k_{sea}$  is the gas transfer  
 337 velocity ( $\text{length time}^{-1}$ ),  $[\text{NO}]$  is the measured concentration of NO in the surface seawater ( $\text{mole volume}^{-1}$ )  
 338  $^1$ ),  $x'\text{NO}_{\text{air}}$  is the mixing ratio of atmosphere NO (dimensionless). And  $p_{ss}$  is the barometric pressure  
 339 while  $p_w$  was calculated after Weiss and Price (1980):

340  $\ln p_w = 24.4543 - 6745.09/(T + 273.15) - 4.8489 \times \ln(T + 273.15)/100 - 0.000544 \times S$  (Eq 8)

341  $H^{cp}$  is the Henry's law constant which is calculated after Sander (2015) as:

342  $H^{cp}(T) = H^\ominus \times \exp(-\Delta sol H/R \times (1/T - 1/T^\ominus))$  (Eq 9)

343 where  $-\Delta sol \frac{H}{R} = \frac{d \ln H}{d \ln(\frac{1}{T})}$ ,  $H^\ominus$ , and  $-\Delta sol H/R$  are tabulated in Sander (2015) ( $-\Delta sol H/R=1600$  and

344  $H^\ominus=1.9 \times 10^{-5}$  mol m<sup>-3</sup> pa<sup>-1</sup>). The reviewed several literatures about NO,  $H^\ominus$  and the values in different  
 345 literatures were similar (Sander, 2015). In our calculation, the value in the Warneck and Williams (2012)  
 346 were used.

347 Then  $k_{sea}$  was calculated after (Wanninkhof, 2014) as (Eq 10),

348  $k_{sea} = k_w (1 - \gamma_a)$  (Eq 10)

349  $\gamma_a$  is the fraction of the entire gas concentration gradient across the airside boundary layer as a fraction  
 350 of the entire gradient from the bulk water to the bulk air (dimensionless),  $k_a$  is the air side air-sea gas  
 351 transfer coefficient (length time<sup>-1</sup>) according to (Mcgillis et al., 2000; Jähne et al., 1987; Sharqawy et al.,  
 352 2010), for the details of the calculation of  $k_w$  and  $\gamma_a$  see Tian et al. (2018).

353 Since onboard wind speeds were not available, ECMWF reanalysis data sets (ERA-5 hourly data) were  
 354 applied. We used a value of  $10^{-11}$  (v/v) for atmospheric NO (Law, 2001). The atmosphere pressure was  
 355 set to 101.325 kPa.

356 Since the measurements [NO] were not available from the cruise we estimated [NO] by assuming that  
 357 (1) NO production is mainly resulting from NO<sub>2</sub><sup>-</sup> photodegradation and (2) the NO photoproduction  $R_{NO}$   
 358 as measured in our irradiation experiment is balanced by the NO scavenging rate  $R_s$  (3) rates of nitrite  
 359 photoproduction into NO was proportional to the irradiance flux in order to adjust the rates under  
 360 simulator light into ambient light at the sampling time (Zafiriou and McFarland, 1981; Olasehinde et al.,  
 361 2010):

362  $R_{NO} \times \frac{I_{ambient}}{I_{simulator}} = [NO] \times R_s,$  (Eq 11)

363 where  $R_s$  represents the sum of the rate constants for the scavenging compounds reacting with NO times  
 364 the concentrations of the scavenger compounds,  $I_{ambient}$  and  $I_{simulator}$  denote the light intensity of  
 365 the sampling station and the CPS+ simulator (765 W m<sup>-2</sup>).  $I_{ambient}$  was ECMWF reanalysis data sets  
 366 (ERA-5 hourly data, interpolation method). In the study of Zafiriou et al., (1980) and Anifowose and  
 367 Sakugawa, (2017), they reviewed the NO lifetime in the different area for the Kurose River (0.05–1.3 s),  
 368 the Seto Inland sea (1.8–20 s), and the central Equatorial Pacific (40–200 s, 170 °E Equatorial regions),

369 which showed an increasing trend from river to open sea. It seemed that NO life time in our study area  
 370 should be most similar to the central Equatorial Pacific. Considering part of our sampling stations were  
 371 in open sea while some stations were close to continent like New Guinea Island and Japan, average  
 372 lifetime about 100 s were applied in our study, however the uncertainty was not reported in the literature,  
 373 but estimated uncertainty about 30% might be appropriate. Tian et al (2018) found that NO concentration  
 374 in the surface water showed no significant difference with that in the bottom water (average depth: 43  
 375 m), so it seems reasonable to estimate the steady state NO concentration with the NO concentration in  
 376 the mixed layer. Then [NO] was estimated to range from 0 to  $292 \times 10^{-12}$  mol L<sup>-1</sup> (0 means that sampling  
 377 time during nighttime), with an average of  $49 \times 10^{-12}$  mol L<sup>-1</sup>, which was consistent with previous results  
 378 in central equatorial Pacific ( $46 \times 10^{-12}$  mol L<sup>-1</sup>), while it was lower than near continent seawater like the  
 379 Seto Inland Sea (up to  $120 \times 10^{-12}$  mol L<sup>-1</sup>) and the Jiaozhou Bay ( $157 \times 10^{-12}$  mol L<sup>-1</sup>), which might be  
 380 because of higher nitrite concentration. NO showed lowest concentration in the Kurose River, which  
 381 might because of less nitrite, and shortest life time might also account for this in river water than in  
 382 seawater (Anifowose and Sakugawa, 2017).

383 In Table 1, the resulting flux density of NO for WTNP ranged from 0 to  $13.9 \times 10^{-12}$  mol m<sup>-2</sup> s<sup>-1</sup>, with an  
 384 average of  $1.8 \times 10^{-12}$  mol m<sup>-2</sup> s<sup>-1</sup>, which is in good agreement with that in central equatorial Pacific (see  
 385 Table 1) while it was lower than that in costal seawater such as the Seto Inland Sea or the Jiaozhou Bay,  
 386 consistent with NO concentration distribution.

### 387 3.6.2 Oceanic photoproduction rates of NO

388 The photoproduction rates from our irradiation experiments were extrapolated to the oceanic  
 389 photoproduction in the WTNP with the equation from (Bange and Uher, 2005; Uher and Andreae, 1996)

$$390 R_{ocean} = R_{NO} \times \left( \frac{I_{ocean}(1 - \exp(-K_D \times MLD))}{I_{ss} \times K_D \times MLD} \right) \quad (\text{Eq 12})$$

391 where  $R_{ocean}$  and  $R_{NO}$  are the photoproduction rates for the ocean mixed layer and seawater irradiation  
 392 experiments, respectively, see Section 3.5.  $I_{ocean}$  and  $I_{ss}$  are the average global irradiance at the surface of  
 393 the ocean mixed layer and the solar simulator used here,  $K_D$  is the light attenuation coefficient and MLD  
 394 is the estimated mixed layer depth at the sampled station.

395  $I_{ocean}$  was set to 185 W m<sup>-2</sup>, while  $I_{ss}$  was 765 W m<sup>-2</sup> in our study (Bange and Uher, 2005; Wu et al.,  
 396 2015). As described above,  $K_{D-354}$  was applied to estimate the MLD. In Smyth (2011),  $K_{D-340}$  to  $K_{D-380}$   
 397 derived from 10% residual light level depths ranged from 0.04 m<sup>-1</sup> to 0.07 m<sup>-1</sup> for our study area, we used

398 the average value of 0.05. The MLD was taken as the layer depth where the temperature was 0.2 °C lower  
399 than the 10 m near-face seawater layer (Montégut, 2004), ranging from 13 – 77 m with an average of 37  
400 m. The resulting average  $R_{\text{ocean}}$  was about  $8.6 \pm 4.9 \times 10^{-12} \text{ mol L}^{-1} \text{ min}^{-1}$  for the WTNP at the time of  
401 our cruise. Besides, the temperature at 20 °C in our laboratory experiment would induce about 10% error  
402 (Fig. 4e).

403 The flux induced by NO photoproduction in the WTNP (NO photoproduction rates divide by MLD,  
404 average:  $13 \times 10^{-12} \text{ mol m}^{-2} \text{ s}^{-1}$ ) were significantly larger than the NO air-sea flux densities (average:  
405  $1.8 \times 10^{-12} \text{ mol m}^{-2} \text{ s}^{-1}$ ) indicating a further NO loss process in the surface layer.

## 406 **Conclusion**

407 The results of our irradiation experiments showed that NO photoproduction from  $\text{NO}_2^-$  in artificial  
408 seawater is significantly affected by changes in pH, temperature and salinity. We found increasing NO  
409 production rates from dissolved  $\text{NO}_2^-$  with decreasing pH, increasing temperatures and increasing  
410 salinity. In contrast we did not find any correlations of NO photoproduction with pH, salinity, water  
411 temperature as well as dissolved  $\text{NO}_2^-$  in natural surface seawater samples from a cruise to the western  
412 tropical North Pacific Ocean (November 2015 – January 2016). We conclude that the trends observed in  
413 our irradiation experiments with artificial seawater do not seem to be representative for WTNP because  
414 of the complex settings of open ocean environments. Moreover, we conclude that future changes of NO  
415 photoproduction due to ongoing environmental changes such as ocean warming and acidification are,  
416 therefore, difficult to predict and need to be tested by irradiation experiments of natural seawater samples  
417 under varying conditions. The flux induced by NO photoproduction in the WTNP (average:  $13 \times 10^{-12}$   
418  $\text{mol m}^{-2} \text{ s}^{-1}$ ) were significantly larger than the NO air-sea flux densities (average:  $1.8 \times 10^{-12} \text{ mol m}^{-2} \text{ s}^{-1}$ )  
419 <sup>1)</sup> indicating a further NO loss process in the surface layer. This indicates a further NO loss process in  
420 the surface layer of the WTNP. In order to decipher and to quantify the NO production and consumption  
421 pathways in the oceanic surface layer more comprehensive laboratory and onboard measurements are  
422 required.

423 **Author contributions.**

424 YT, GY, CL, HC and PL prepared the original manuscript and designed the experiments; HB made many  
425 modifications and gave a lot of suggestions on design of figures and the computing method. All authors  
426 contributed to the analysis of the data and discussed the results.

427 **Competing interests.**

428 The authors declare that they have no conflict of interest.

429 **Acknowledgement**

430 We thank the captain and crew of the R/V “Dong Fang Hong 2” for their support and help during the  
431 cruise. This research was supported by the National Natural Science Foundation of China  
432 (Nos.41676065), the National Key Research and Development Program of China (Grant No.  
433 2016YFA0601301), and the Fundamental Research Funds for the Central Universities (No. 201762032).

434 **References**

- 435 Anifowose, A. J., Takeda, K., and Sakugawa, H.: Photoformation rate, steady-state concentration and  
436 lifetime of nitric oxide radical (NO $\cdot$ ) in a eutrophic river in Higashi-Hiroshima, Japan,  
437 *Chemosphere*, 119, 302-309, 2015.
- 438 Anifowose, A. J., and Sakugawa, H.: Determination of Daytime Flux of Nitric Oxide Radical (NO $\cdot$ ) at  
439 an Inland Sea-Atmospheric Boundary in Japan, *J. Aquat. Pollut. Toxicol.*, 1, 1-6, 2017.
- 440 Astier, J., Jeandroz, S., and Wendehenne, D.: Nitric oxide synthase in plants: The surprise from algae,  
441 *Plant Sci.*, 268, 64-66, 2018.
- 442 Bajt, O., Šket, B., and Faganeli, J.: The aqueous photochemical transformation of acrylic acid, *Mar.*  
443 *Chem.*, 58, 255-259, 1997.
- 444 Bange, H. W., and Uher, G.: Photochemical production of methane in natural waters: implications for its  
445 present and past oceanic source, *Chemosphere*, 58, 177-183, 2005.
- 446 Bange, H. W.: Gaseous Nitrogen Compounds (NO, N $_2$ O, N $_2$ , NH $_3$ ) in the Ocean, Elsevier 51–94 pp.,  
447 2008.
- 448 Benedict, K. B., Mcfall, A. S., and Anastasio, C.: Quantum Yield of Nitrite from the Photolysis of  
449 Aqueous Nitrate above 300 nm, *Environ. Sci. Technol.*, 51, 4387-4395, 2017.
- 450 Chu, L., and Anastasio, C.: Temperature and wavelength dependence of nitrite photolysis in frozen and  
451 aqueous solutions, *Environ. Sci. Technol.*, 41, 3626-3632, 2007.
- 452 Clarke, K., Edge, R., Johnson, V., Land, E. J., Navaratnam, S., and Truscott, T. G.: The carbonate radical:  
453 its reactivity with oxygen, ammonia, amino acids, and melanins, *J. Phys. Chem. A*, 112, 10147-  
454 10151, 2008.



455 Fine, R. A., Lukas, R., Bingham, F. M., Warner, M. J., and Gammon, R. H.: The western equatorial  
456 Pacific: A water mass crossroads, *J. Geophys. Res.: Oceans*, 99, 25063-25080, 1994.

457 Goldstein, S., and Rabani, J.: Mechanism of Nitrite Formation by Nitrate Photolysis in Aqueous  
458 Solutions: The Role of Peroxynitrite, Nitrogen Dioxide, and Hydroxyl Radical, *J. Am. Chem.*  
459 *Soc.*, 129, 10597, 2007.

460 Jähne, B., Heinz, G., and Dietrich, W.: Measurement of the diffusion coefficients of sparingly soluble  
461 gases in water, *J. Geophys. Res.: Oceans*, 92, 10767–10776, 1987.

462 Jousotdubien, J., and Kadiri, A.: Photosensitized Oxidation of Ammonia by Singlet Oxygen in Aqueous  
463 Solution and in Seawater, *Nature*, 227, 700-701, 1970.

464 Kieber, D. J., Jiao, J., Kiene, R. P., and Bates, T. S.: Impact of dimethylsulfide photochemistry on methyl  
465 sulfur cycling in the Equatorial Pacific Ocean, *J. Geophys. Res.: Oceans*, 101, 3715-3722, 1996.

466 Kieber, R. J., Li, A., and Seaton, P. J.: Production of nitrite from the photodegradation of dissolved  
467 organic matter in natural waters, *Environ. Sci. Technol.*, 33, 717-723, 1999.

468 Kuypers, M. M. M., Marchant, H. K., and Kartal, B.: The microbial nitrogen-cycling network, *Nat. Rev.*  
469 *Microbiol.*, 16, 263-276, 2018.

470 Lantoiné, F., Trévin, S., Bedioui, F., and Devynck, J.: Selective and sensitive electrochemical  
471 measurement of nitric oxide in aqueous solution: discussion and new results, *J. Electroanal.*  
472 *Chem.*, 392, 85-89, 1995.

473 Laszlo, B., Alfassi, Z. B., Neta, P., and Huie, R. E.: Kinetics and Mechanism of the Reaction of  $\bullet\text{NH}_2$   
474 with  $\text{O}_2$  in Aqueous Solutions, *J. Phys. Chem. A*, 102, 8498-8504, 1998.

475 Law, C. S.: Air–sea transfer:  $\text{N}_2\text{O}$ ,  $\text{NO}$ ,  $\text{CH}_4$ ,  $\text{CO}$ , *Encyclopedia of Ocean Sciences*, 137-144, 2001.

476 Li, P. F., Li, W. S., Liu, C. Y., Zhu, X. C., and Zhang, Q.: The photodecomposition of nitrite in water (in  
477 Chinese), *Chin. J. Environ. Sci.*, 30, 1883-1888, 2011.

478 Li, Y., Mao, Y., Liu, G., Tachiev, G., Roelant, D., Feng, X., and Cai, Y.: Degradation of methylmercury  
479 and its effects on mercury distribution and cycling in the Florida Everglades, *Environ. Sci.*  
480 *Technol.*, 44, 6661-6666, 2010.

481 Liu, C. Y., Feng, W. H., Tian, Y., Yang, G. P., Li, P. F., and Bange, H. W.: Determination of dissolved  
482 nitric oxide in coastal waters of the Yellow Sea off Qingdao, *Ocean Sci.*, 13, 623-632, 2017.

483 Lutterbeck, H. E., and Bange, H. W.: An improved method for the determination of dissolved nitric oxide  
484 (NO) in seawater samples, *Ocean Sci.*, 11, 959-981, 2015.

485 Mack, J., and Bolton, J. R.: Photochemistry of nitrite and nitrate in aqueous solution: a review, *J.*  
486 *Photochem. Photobiol.*, A, 128, 1-13, 1999.

487 McGillis, W. R., Dacey, J. W. H., Frew, N. M., Bock, E. J., and Nelson, R. K.: Water-air flux of  
488 dimethylsulfide, *J. Geophys. Res.: Oceans*, 105, 1187–1193, 2000.

489 Minero, C., Chiron, S., Falletti, G., Maurino, V., Pelizzetti, E., Ajassa, R., Carlotti, M. E., and Vione, D.:  
490 Photochemical processes involving nitrite in surface water samples, *Aquat. Sci.*, 69, 71-85,  
491 2007.

492 Montégut, C. D. B.: Mixed layer depth over the global ocean: An examination of profile data and a  
493 profile-based climatology, *J. Geophys. Res.: Oceans*, 109, -, 2004.

494 Olasehinde, E. F., Takeda, K., and Sakugawa, H.: Development of an analytical method for nitric oxide  
495 radical determination in natural waters, *Anal. Chem.*, 81, 6843-6850, 2009.

496 Olasehinde, E. F., Takeda, K., and Sakugawa, H.: Photochemical Production and Consumption  
497 Mechanisms of Nitric Oxide in Seawater, *Environ. Sci. Technol.*, 44, 8403-8408, 2010.

498 Sander, R.: Compilation of Henry's law constants (version 4.0) for water as solvent, *Atmos. Chem. Phys.*,  
499 14, 29615-30521, 2015.

500 Schreiber, F., Wunderlin, P., Udert, K. M., and Wells, G. F.: Nitric oxide and nitrous oxide turnover in  
501 natural and engineered microbial communities: biological pathways, chemical reactions, and  
502 novel technologies, *Front. Microbiol.*, 3, 372, 2012.

503 Sharqawy, M. H., V, J. H. L., and Zubair, S. M.: Thermophysical properties of seawater: a review of  
504 existing correlations and data, *Desalin. Water Treat.*, 16, 354-380, 2010.

505 Singh, V. K., and Lal, B.: Nitric oxide (NO) stimulates steroidogenesis and folliculogenesis in fish,  
506 *Reproduction*, 153, 133, 2016.

507 Smyth, T. J.: Penetration of UV irradiance into the global ocean, *J. Geophys. Res.: Oceans*, 116, 20-32,  
508 2011.

509 Tian, Y., Xue, C., Liu, C. Y., Yang, G. P., Li, P. F., Feng, W. H., and Bange, H. W.: Nitric oxide (NO)  
510 in the Bohai and Yellow Seas, *Biogeosciences Discuss.*(DOI: 10.5194/bg-2018-446), 2018, 1-  
511 25, 2018.

512 Tugaoen, H. O. N., Herckes, P., Hristovski, K., and Westerhoff, P.: Influence of ultraviolet wavelengths  
513 on kinetics and selectivity for N-gases during TiO<sub>2</sub> photocatalytic reduction of nitrate, *Appl.*  
514 *Catal., B*, 220, 597-606, 2018.

515 Uher, G., and Andreae, M. O.: The diel cycle of carbonyl sulfide in marine surface waters: Field study  
516 results and a simple model, *Aquatic Geochemistry*, 2, 313-344, 1996.

517 Wang, B., Dan, L., Chao, W., Wang, Q., Hui, Z., Liu, G., Xia, T., and Zhang, L.: Mechanism of  
518 endothelial nitric oxide synthase phosphorylation and activation by tentacle extract from the  
519 jellyfish *Cyanea capillata*, *Peerj*, 5, e3172, 2017.

520 Wanninkhof, R.: Relationship between wind speed and gas exchange over the ocean revisited, *Limnol.*  
521 *Oceanogr. Methods*, 12, 351-362, 2014.

522 Weiss, R. F., and Price, B. A.: Nitrous oxide solubility in water and seawater, *Mar. Chem.*, 8, 347-359,  
523 1980.

524 Wu, X., Liu, C. Y., and Li, P. F.: Photochemical transformation of acrylic acid in seawater, *Mar. Chem.*,  
525 170, 29-36, 2015.

526 Xing, L., Zhang, Z. B., Liu, C. Y., Wu, Z. Z., and Lin, C.: Amperometric Detection of Nitric Oxide with  
527 Microsensor in the Medium of Seawater and Its Applications, *Sensors*, 5, 537-545, 2005.

528 Xue, C., Liu, C., Yang, G., Zhu, C., and Zhang, H.: Distribution and controlling factors of nitric oxide  
529 concentrations in surface seawater of Jiaozhou Bay and adjacent waters (in Chinese), *Chin. J.*  
530 *Environ. Sci.*, 33, 1086-1090, 2012.

531 Yang, G. P., Ren, C. Y., Lu, X. L., Liu, C. Y., and Ding, H. B.: Distribution, flux, and photoproduction  
532 of carbon monoxide in the East China Sea and Yellow Sea in spring, *J. Geophys. Res.: Oceans*,  
533 116, 1-15, 2011.

534 Zafiriou, O. C., and True, M. B.: Nitrite photolysis in seawater by sunlight ☆, *Mar. Chem.*, 8, 33-42,  
535 1979.

536 Zafiriou, O. C., McFarland, M., and Bromund, R. H.: Nitric oxide in seawater, *Science*, 207, 637, 1980.

537 Zafiriou, O. C., and McFarland, M.: Nitric oxide from nitrite photolysis in the central equatorial Pacific,  
538 *J. Geophys. Res.: Oceans*, 86, 3173-3182, 1981.

539 Zellner, R., Exner, M., and Herrmann, H.: Absolute OH quantum yields in the laser photolysis of nitrate,  
540 nitrite and dissolved H<sub>2</sub>O<sub>2</sub> at 308 and 351 nm in the temperature range 278-353 K, *J. Atmos.*  
541 *Chem.*, 10, 411-425, 1990.

542 Zhang, Z., Qiu, B., Tian, J., Zhao, W., and Huang, X.: Latitude-dependent finescale turbulent shear  
543 generations in the Pacific tropical-extratropical upper ocean, *Nat. Commun.*, 9, 4086, 2018.

544 Zhao, J., Li, Y., and Wang, F.: Seasonal variation of the surface North Equatorial Countercurrent (NECC)  
545 in the western Pacific Ocean, *Chin. J. Oceanol. Limnol.*, 34, 1332-1346, 2016.

546 Zhu, W. Z., Zhang, J., and Yang, G. P.: Mixing behavior and photobleaching of chromophoric dissolved  
547 organic matter in the Changjiang River estuary and the adjacent East China Sea, *Estuarine,  
548 Coastal Shelf Sci.*, 2017.

549

550

## Figure Captions

551

552 **Fig. 1.** Locations of the sampling stations in the western tropical North Pacific Ocean. The acronyms  
553 NGCC, SEC, NECC, NEC, and STCC stand for New Guinea Coastal Current, South Equatorial Current,  
554 North Equatorial Counter Current, North Equatorial Current, and Subtropical Counter Current,  
555 respectively.

556 **Fig. 2.** Changes of NO concentrations with initial DAF-2 concentration of 0, 0.7, 1.4, 2.1, 2.8, 3.5 and  
557 4.2  $\mu\text{mol L}^{-1}$  after irradiation time of 2 h (a) and changes of different NO concentrations with storage  
558 time monitored at about 2 h time intervals (b).

559 **Fig. 3.** Photoproduction rates of NO with 0.5, 2, and 5.0  $\mu\text{mol L}^{-1}$   $\text{NO}_2^-$  (a) and the calculated  $J_{\text{NO}}$  values  
560 in Milli-Q water and artificial seawater (b), symbols in red represented for the artificial seawater samples  
561 and in black for Milli-Q water.

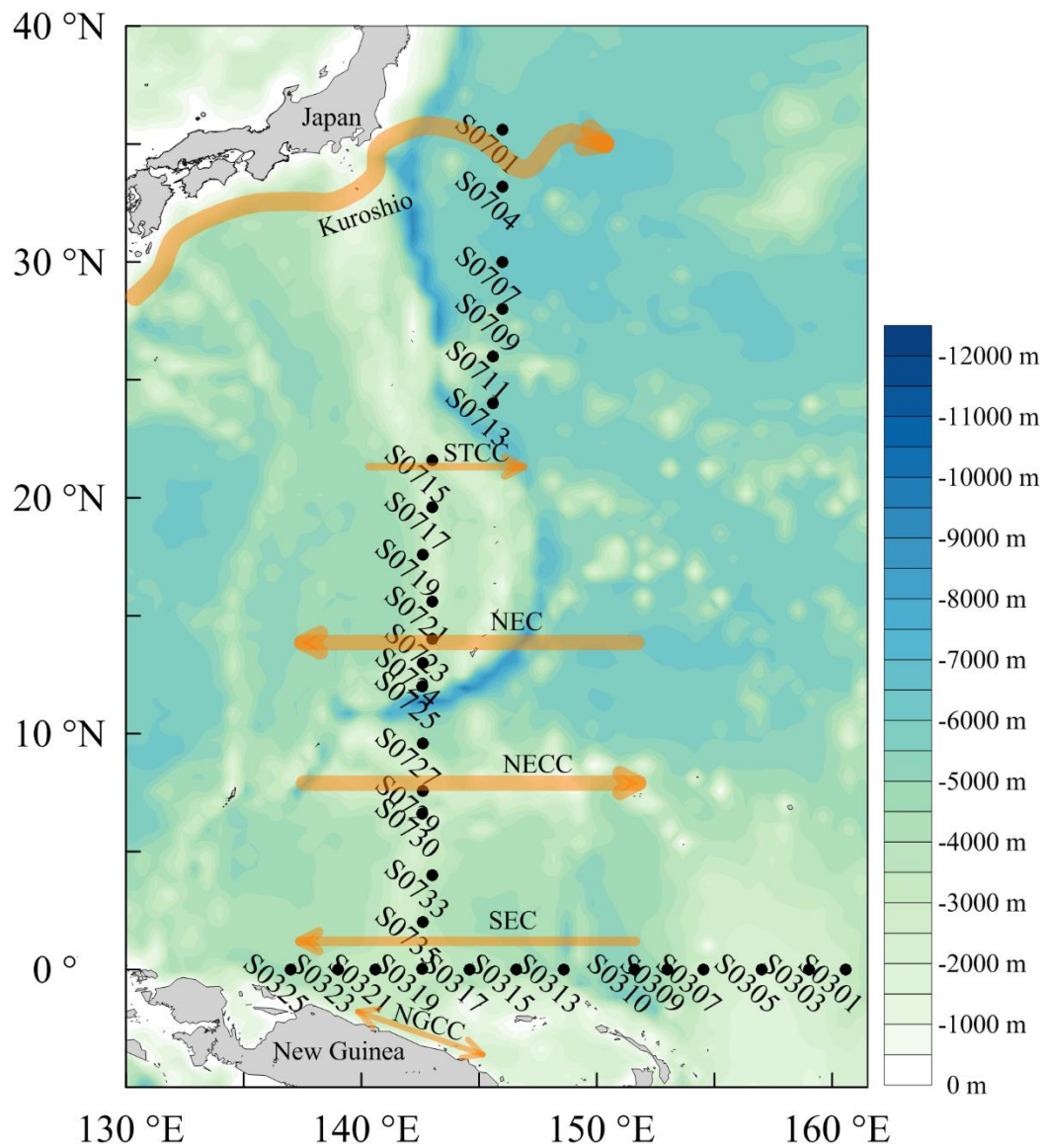
562 **Fig. 4.** NO concentration changes with irradiation time at different pH, salinity, temperature and  
563 waveband conditions (a, c, e, g for 0.5  $\mu\text{mol L}^{-1}$   $\text{NO}_2^-$  and b, d, f, h for 5.0  $\mu\text{mol L}^{-1}$   $\text{NO}_2^-$ ).

564 **Fig. 5.** Changes of NO photoproduction rates with irradiation time at different pH, salinity, temperature  
565 and waveband conditions (a, c, e, g for 0.5  $\mu\text{mol L}^{-1}$   $\text{NO}_2^-$  and b, d, f, h for 5.0  $\mu\text{mol L}^{-1}$   $\text{NO}_2^-$ ).

566 **Fig. 6.** Seawater temperature, salinity, concentrations of  $\text{NO}_2^-$ ,  $\text{NO}_3^-$ ,  $\text{NH}_4^+$ , and photoproduction rates  
567 of NO ( $R_{\text{NO}}$ ) in the western tropical North Pacific Ocean. (a: W/E transect; b: N/S transect)

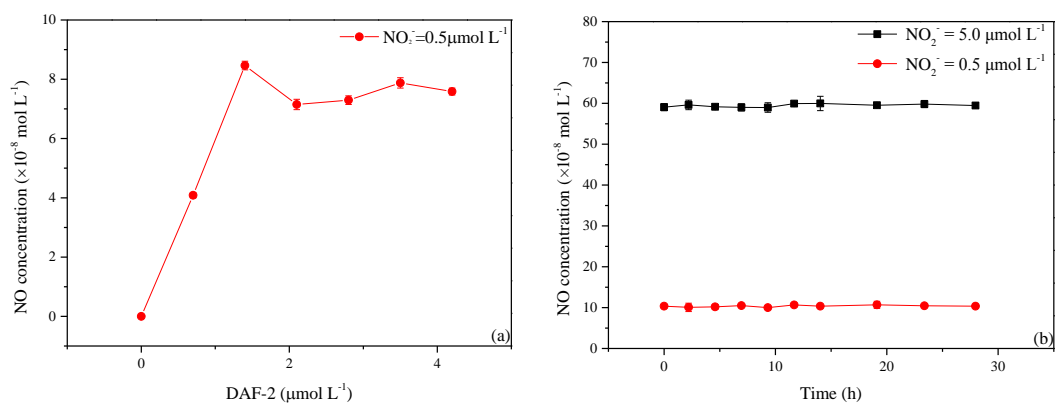
568 **Fig. 7.** The potential temperature–salinity (T–S) diagram with NO photoproduction rates indicated in the  
569 color bar. Water mass characteristics of surface currents shown in Figure 1 are indicated. The acronyms  
570 NGCC, SEC, NECC, NEC, and STCC stand for New Guinea Coastal Current, South Equatorial Current,  
571 North Equatorial Counter Current, North Equatorial Current, and Subtropical Counter Current,  
572 respectively.





574  
 575  
 576  
 577  
 578  
 579  
 580

**Fig. 1.** Locations of the sampling stations in the western tropical North Pacific Ocean. The acronyms NGCC, SEC, NECC, NEC, and STCC stand for New Guinea Coastal Current, South Equatorial Current, North Equatorial Counter Current, North Equatorial Current, and Subtropical Counter Current, respectively.



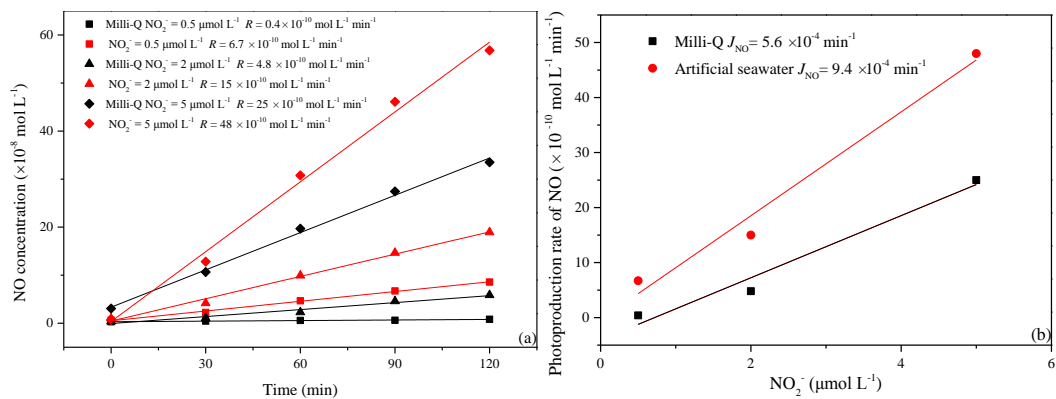
581

582 **Fig. 2.** Changes of NO concentrations with initial DAF-2 concentration of 0, 0.7, 1.4, 2.1, 2.8, 3.5 and

583 4.2  $\mu\text{mol L}^{-1}$  after irradiation time of 2 h (a) and changes of different NO concentrations with storage

584 time monitored at about 2 h time intervals (b).

585



586

587

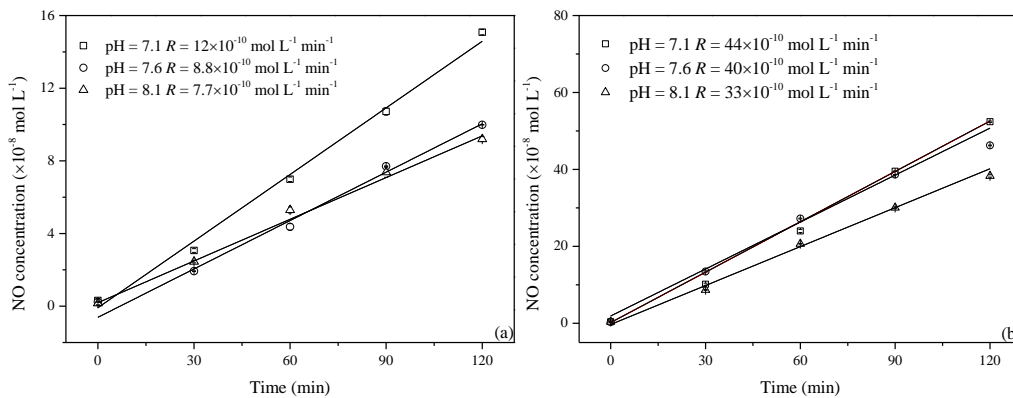
588 **Fig. 3.** Photoproduction rates of NO with 0.5, 2, and 5.0  $\mu\text{mol L}^{-1} \text{NO}_2^-$  (a) and the calculated  $J_{\text{NO}}$

589 values in Milli-Q water and artificial seawater (b), symbols in red represented for the artificial

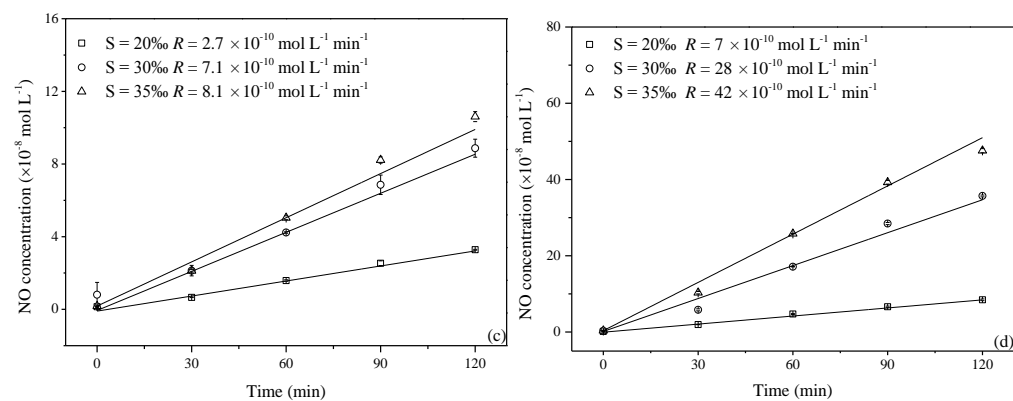
590 seawater samples and in black for Milli-Q water.

591

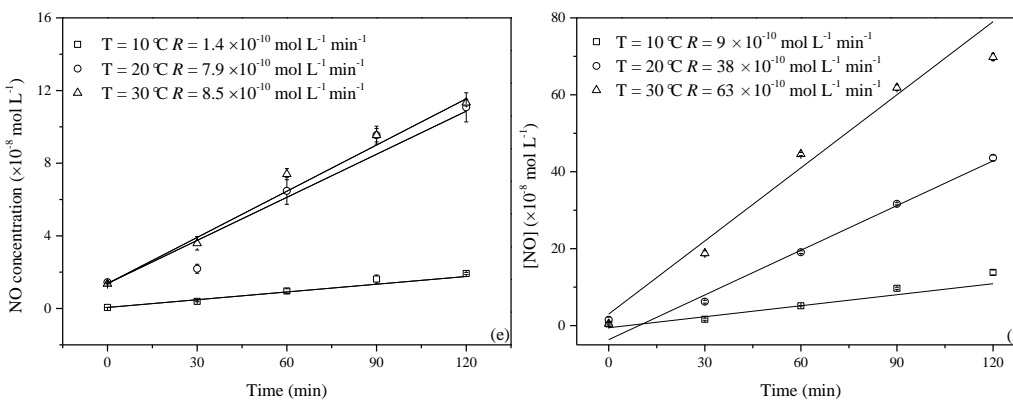




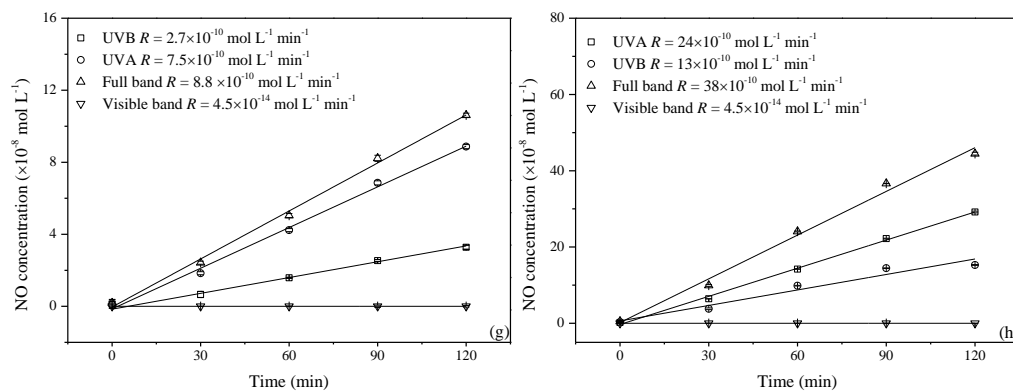
592



593



594

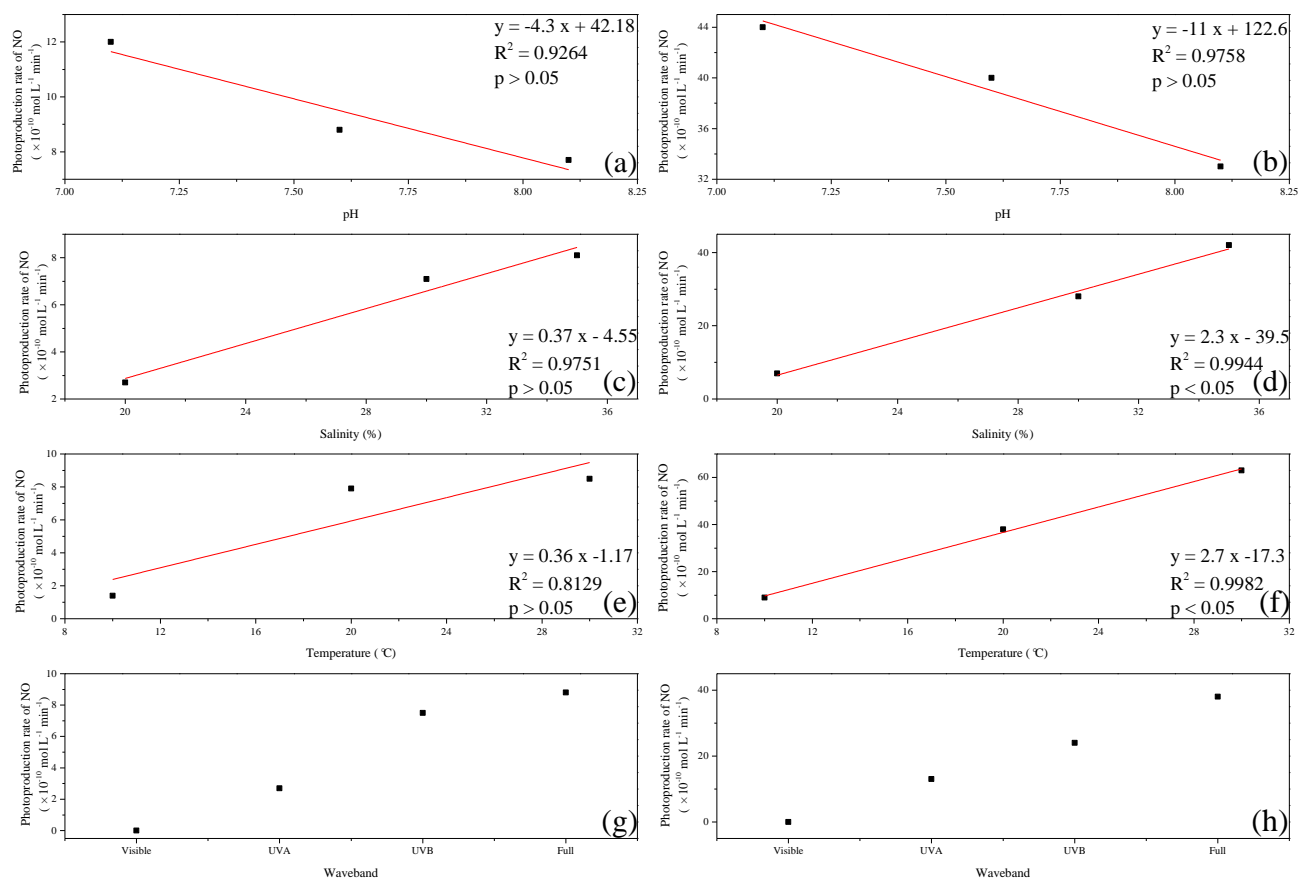


595

596 **Fig. 4.** NO concentration changes with irradiation time at different pH, salinity, temperature and

597 waveband conditions (a, c, e, g for  $0.5 \mu\text{mol L}^{-1} \text{NO}_2^-$  and b, d, f, h for  $5.0 \mu\text{mol L}^{-1} \text{NO}_2^-$ ).

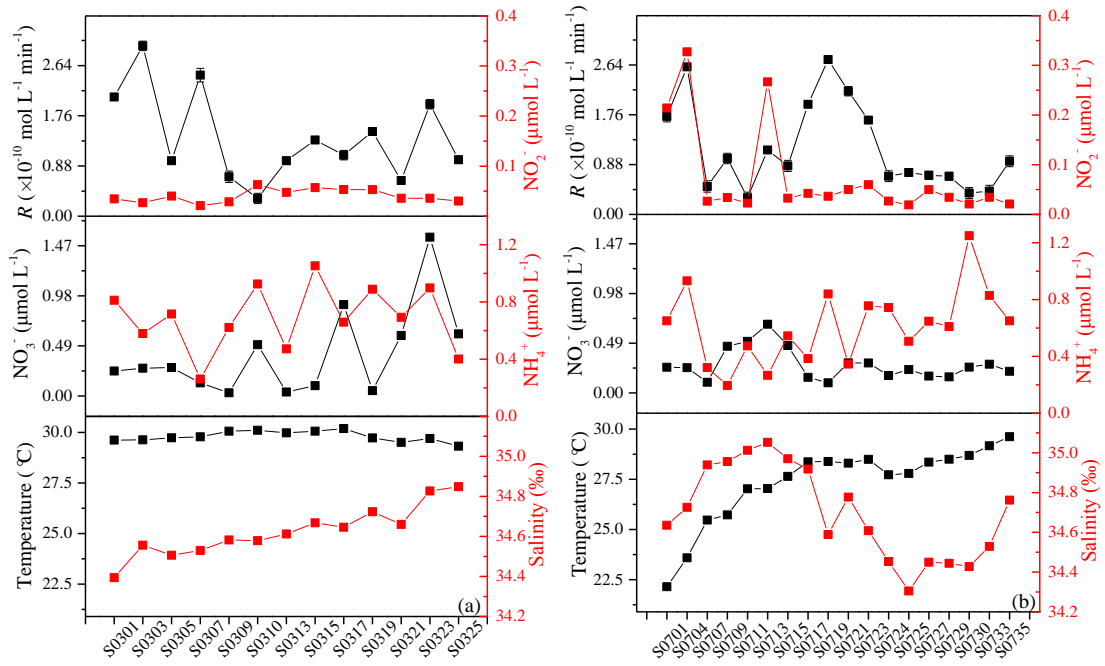
598



600

601 **Fig. 5.** Changes of NO photoproduction rates with irradiation time at different pH, salinity, temperature602 and waveband conditions (a, c, e, g for  $0.5 \mu\text{mol L}^{-1} \text{NO}_2^-$  and b, d, f, h for  $5.0 \mu\text{mol L}^{-1} \text{NO}_2^-$ ).

603

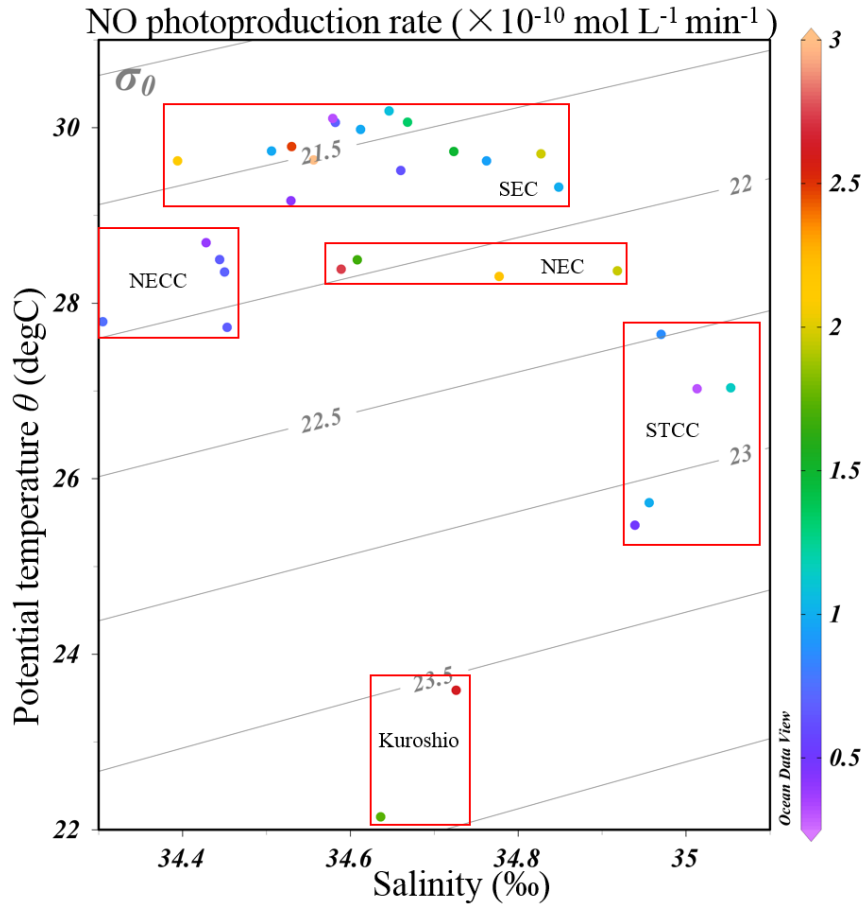


604

605 **Fig. 6.** Seawater temperature, salinity, concentrations of  $\text{NO}_2^-$ ,  $\text{NO}_3^-$ ,  $\text{NH}_4^+$ , and photoproduction

606 rates of NO ( $R_{\text{NO}}$ ) in the western tropical North Pacific Ocean (a: W/E transect; b: N/S transect.).

607



608

609 **Fig. 7.** The potential temperature–salinity (T–S) diagram with NO photoproduction rates indicated in  
 610 the color bar. Water mass characteristics of the surface currents shown in Figure 1 are indicated. The  
 611 acronyms NGCC, SEC, NECC, NEC, and STCC stand for New Guinea Coastal Current, South  
 612 Equatorial Current, North Equatorial Counter Current, North Equatorial Current, and Subtropical  
 613 Counter Current, respectively.

614

615

### Table Captions

616 **Table 1** Photoproduction rates ( $R$ ), average NO concentrations and average flux densities of NO in  
617 different regions.

618 **Table 2** The ratios of photoproduction rates ( $R_{5.0}/R_{0.5}$ ) in the different irradiation experiments.

619

620 **Table 1** Photoproduction rates (*R*), average NO concentrations, NO<sub>2</sub><sup>-</sup> concentrations and average flux  
 621 densities of NO in different regions.

Regions	<i>R</i> (mol L <sup>-1</sup> s <sup>-1</sup> )	NO (mol L <sup>-1</sup> )	NO <sub>2</sub> <sup>-</sup> μmol L <sup>-1</sup>	Flux (mol m <sup>-2</sup> s <sup>-1</sup> )	Sampling date	References
Seto Inland Sea, Japan	8.7–38.8×10 <sup>-12</sup>	120×10 <sup>-12</sup>	0.5-2	3.55×10 <sup>-12</sup>	October 5–9, 2009	Olasehinde et al., 2010
Seto Inland Sea, Japan	1.4-9.17×10 <sup>-12</sup>	3-41×10 <sup>-12</sup>	0-0.4	0.22 ×10 <sup>-12</sup>	September, 2013 and June, 2014	Anifowose and Sakugawa, 2017
Kurose River, Japan	9.4–300×10 <sup>-12</sup>	–	-	–	–	Olasehinde et al., 2009
Kurose River (K1 station), Japan	4×10 <sup>-12</sup>	1.6×10 <sup>-12</sup>	0.06	–	Monthly, 2013	Anifowose et al., 2015
Jiaozhou Bay	–	157×10 <sup>-12</sup>	-	7.2×10 <sup>-12</sup>	June, July and August, 2010	Tian et al., 2016
Jiaozhou Bay and its adjacent waters	–	(160 ± 130)×10 <sup>-12</sup>	-	10.9×10 <sup>-12</sup>	March 8–9, 2011	Xue et al., 2011
Coastal water off Qingdao	1.52 ×10 <sup>-12</sup>	260×10 <sup>-12</sup>	0.75	-	November, 2009	Liu et al., 2017
Central equatorial Pacific	> 10 <sup>-12</sup>	46×10 <sup>-12</sup>	0.2	2.2×10 <sup>-12</sup>	R/V Knorr 73/7	Zafiriou and Mcfarland., 1981
The northwest Pacific Ocean	0.5 ± 0.2×10 <sup>-12</sup>	49×10 <sup>-12</sup>	0.06	1.8×10 <sup>-12</sup>	November 15, 2015 to January 26, 2016	This study

622

623 **Table 2** The ratios of photoproduction rates ( $R_{5.0}/R_{0.5}$ ) in the different irradiation experiments.

	$R (\times 10^{-10} \text{ mol L}^{-1} \text{ min}^{-1})$		Ratio
	0.5 $\mu\text{M}$	5.0 $\mu\text{M}$	
pH=7.1	12	44	3.7
pH=7.6	8.8	40	4.5
pH=8.1	7.7	33	4.3
T=10 °C	1.4	9.0	6.4
T=20 °C	7.9	38	4.8
T=30 °C	8.5	63	7.4
S=20	2.7	7.0	2.6
S=30	7.1	28	3.9
S=35	8.1	42	5.2

624